Experimental and Numerical Investigation on the performance characteristics of Flat Coil tube Water Solar Collector

Kadhim Fadhil Nasir
Farm Machinery and Equipment Eng. Dept., AL Furat Alawsat Technical University –AL Mussaib Technical College
kka_ff70@yahoo.com

Abstract

Experimental and numerical investigation of using flat coiled tube as a receiver in a tilted Flat Coil Solar Collector (FCSC) for heating water is presented in the present work. The test rig is designed, constructed, and tested with stationary north-south direction tracking system. All experimental tests are done outdoor conditions at AL-Mussaib-Babylon Iraq (Latitude of 32.5° North and Longitude of 44.3° East) at a tilt angle of 32.5° with horizontal for a period of March and April 2015. Variable water volume flow rates are used through the receiver for 11 clear and partly cloudy days on March 2015, then replication on April 2015. The numerical investigation involves a numerical solution of two models for flat coiled tube by a commercial package ANSYS FLUENT 15.0. Boundary conditions of each model that solved are taken from experimental tests. The experimental results gained of experimental tests indicated that a maximum temperatures difference between outlet and inlet of receiver and the maximum useful heat gain are 4º C, 1300 W, respectively. The maximum water temperature at receiver outlet is 72 ºC. It showed that the maximum temperature in the storage tank is 71 ºC for clear day. The maximum collector efficiency is 81.6 %. The numerical results obtained by solution of models obtainable the static temperature and pressure contours, also it showed the temperature difference between outlet and inlet of receiver and the collector thermal efficiency are agreement with experimental results. The present experimental results compared with available previous studies for flat plate solar collector and gave best results for the present work; represented by 12.3 % enchainment in the storage water temperature.

Key words: solar, flat, plate, collector, thermal, efficiency, water, temperature, heat, energy.

الخلاصة

تضمن البحث الحالي دراسة عملية لاستخدام انبوب ملفوف سطحيا كمستقبل شمسي لمجمع شمسي مسطح مائل من اجل الحصول على ماء ساخن. تم تصميم وبناء واختبار هذا المجمع الشمسي بدون استخدام منظومة توجيه . انجزت الدراسة العملية في الاجواء الخارجية بمدينة المسيب– محافظة بابل– العراق (خط عرض 32.5° شمالا وخط طول 44.3° شرقا) عند زاوية ميلان 32.5° مع الافق خلال شهري اذارونيسان 2015 . استخدمت معدلات تدفق متغيرة للماء. الدراسة النظرية تضمنت عمل محاكات باستخدام برنامج ANSYS FLUENT 15.0 لنموذجين من الانابيب الملفوفة سطحيا، الظروف الحدية للنموذجين اخذت من التجارب العملية. اظهرت النتائج المستحصلة من الاختبارات العملية ان اعظم فرق لدرجات الحرارة مابين مدخل ومخرج المستقبل الشمسي واعظم كمية حرارة مستحصلة كانت 4 °C و 1300 واط على التوالي. واظهرت اعظم درجة حرارة للماء الخارج من المستقبل الشمسي هي72 °C واعظم درجة حرارة للماء داخل الخزان المعزول في طقس صحو كانت 71 °C. اعظم كفاءة حرارية للمجمع الشمسي التي تم الحصول عليها ع هي 81.6% . اظهرت النتائج النظرية تطابقا مع النتائج العملية لفرق درجات حرارة الماء والكفاءة الحرارية. تم مقارنة النتائج العملية لهذه الدراسة مع نتائج بحوث سابقة للمجمعات الشمسية السطحية وقد اظهرت المقارنة افضلية جيدة في النتائج للمجمع الشمسي الحالي بنسبة 12.3% زيادة في درجة حرارة الماء المخزون.

كلمات المفتاحية:– الاشعاع الشمسي، صفيحه، مستوي، مجمع شمسي، كفاءة، حرارية، ماء، درجة حرارة، طاقة حرارية.

1. Introduction

Solar energy collectors are mediums commonly designed for collecting and absorbed solar energy radiation. The absorbed solar energy radiation is transformed into heat energy by collectors which are finally transferred into the working fluid of the system generally water or air which the common working fluid. Mainly, there are two types of solar collectors: stationary and sun tracking or concentrating solar collectors (Soteris, 2004). Solar heating water systems play an animated role in low temperature applications especially in daily using at homes and hotels. Solar collector absorbs the received solar radiation energy, then converting to a thermal energy at an absorbing surface, finally the energy transferred to a flowing fluid through the

collector. This fluid may be using for various purposes such heating the building and to dry the agricultural products etc. The solar energy is clean source environmentally of energy and it is free and obtainable in suitable quantities in the world where people live. Solar radiation flux available in the hottest regions on earth rarely exceeds 1 kW/sq-m (Madhukeshwara *et.al.,* 2012). Many research works have been reported in the literature on harvesting energy from solar; (Duffie and Beckman, 1991) developed a model for the flat plate heating solar collector which is widely used for design and prediction. Heat transfer assumed one dimensional from the hot fluid to the ambient. Temperature at the absorber, covers and back plate are considered with steady state fluid conditions from the analogy between electrical grids and one dimensional heat transfer. A transient three dimensions mathematical model for flat plate heating solar collector is developed by (Villar *et.al.,* 2009). Energy and mass balances was considered in model solution by finite volumes. The model employed different configurations. Insulation of transparent honeycomb between cover and plate also modeled. The temperature effect on the materials thermal properties considered. The model validated experimentally and considers a useful tool for developing the design of plate solar collector and for comparison different configurations. (Cadafalch, 2009) developed a one dimensional numerical transient model of flat heating plate solar devices. The model considerations includes; the analysis of different configurations and parts as multi glass cover, gaps of air, transparent insulation, opaque insulation, the surface coatings, and energy growth in water or phase change material. The results show comparisons of numerical and experimental and gave good validation.. (Hobbi and Siddiqui, 2009) studied the effect of heat transfer enhancement devices upon thermal performance for the flat plate solar collector experimentally. Many passive heat transfer enhancement devices which include coil-spring wire, twisted strip, and conical ridges are studied. (Sekhar *et.al.,* 2009) investigated the evaluation of the top losses coefficient of the flat plate collector theoretically and experimentally. Theoretical and experimental analysis was performed with a single cover of glass for a flat plate collector. It concluded that the absorber plate emissivity has a important effect on a top losses coefficient of flat plate collector. The thermal efficiency values of flat plate collector are established to increase with the increasing of ambient temperature. (Mahmud *et.al.,* 2016) used nanofluids as heat transfer fluids to enhance the performance of solar collector devices; flat-plate and evacuated tube solar collectors and evaluated efficiency of solar collectors with nanofluids, also discussed the impact of nanofluids in solar collectors on economic and environmental. The aim of this work can be indicated in the experimental and theoretical studies to evaluate the hydrothermal performance of the flat coiled copper tube that used as receiver of solar collector in Iraq environment.

NOMENCLATURE

Symbol	**Definition**	**Units**	**Symbol**	**Definition**	**Units**
A	Area, apparent	m^2	$\dot{m}$	Mass flow rate	Kg/s
C_p	Specific heat	J/kg.k	Greek symbols		
d	Diameter of the tube	m	ρ	density	Kg/ m^3
f_c	Friction Factor		η	Efficiency of collector	
I	Incident solar radiation,	W/m^2	ΔP	Pressure Drop	KPa

L	Tube length	m	Subscripts		
Q	Heat transfer rate	W	a	Air, ambient, aperture	
Q_u	Useful energy gained from collector	W	i	Inlet	
T	Temperature	°C	o	Outlet	
V	velocity	m/s			

2. Numerical Analysis

The geometry of the receiver (flat coiled tube) is created in ANSYS-FLUENT-15. A cylindrical polar coordinate system (r, θ, z) is used is shown in figure (1a) with a mesh size of 434573 nodes and 433368 elements. The minimum size of cell in a mesh is $5.7075*10^{-4}$ m, maximum size of $0.11415*10^{-2}$ m, and maximum face size is $5.7075*10^{-2}$ m which shown in figures (1b). The continuity equation, momentum equation, and energy equation are (Bird *et.al.*, 1987, Bird *et.al.*, 2002) :

Continuity equation

$$\frac{1}{r}\frac{\partial(\rho r v_r)}{\partial r}+\frac{1}{r}\frac{\partial(\rho v_\theta)}{\partial \theta}+\frac{\partial(\rho v_z)}{\partial z}=0 \text{----------(1)}$$

Momentum equation

r-

$$v_r\frac{\partial v_r}{\partial r}+\frac{v_\theta}{r}\frac{\partial v_r}{\partial \theta}+v_z\frac{\partial v_r}{\partial r}-\frac{{v_\theta}^2}{r}=-\frac{1}{\rho}\frac{\partial p}{\partial r}+\frac{\mu}{\rho}\left(\frac{1}{r}\frac{\partial}{\partial r}\left(r\frac{\partial v_r}{\partial r}\right)+\frac{1}{r^2}\frac{\partial^2 v_r}{\partial \theta^2}+\frac{\partial^2 v_r}{\partial z^2}-\frac{v_r}{r^2}-\frac{2}{r^2}\frac{\partial v_\theta}{\partial \theta}\right) \text{---(2)}$$

θ-

$$v_r\frac{\partial v_\theta}{\partial r}+\frac{v_\theta}{r}\frac{\partial v_\theta}{\partial \theta}+v_z\frac{\partial v_\theta}{\partial r}+\frac{v_r v_\theta}{r}=-\frac{1}{\rho}\frac{\partial p}{\partial \theta}+\frac{\mu}{\rho}\left(\frac{1}{r}\frac{\partial}{\partial r}\left(r\frac{\partial v_\theta}{\partial r}\right)+\frac{1}{r^2}\frac{\partial^2 v_\theta}{\partial \theta^2}+\frac{\partial^2 v_\theta}{\partial z^2}-\frac{v_\theta}{r^2}+\frac{2}{r^2}\frac{\partial v_r}{\partial \theta}\right) \text{- (3)}$$

z-

$$v_r\frac{\partial v_z}{\partial r}+\frac{v_\theta}{r}\frac{\partial v_z}{\partial \theta}+v_z\frac{\partial v_z}{\partial z}=-\frac{1}{\rho}\frac{\partial p}{\partial z}+\frac{\mu}{\rho}\left(\frac{1}{r}\frac{\partial}{\partial r}\left(r\frac{\partial v_z}{\partial r}\right)+\frac{1}{r^2}\frac{\partial^2 v_z}{\partial \theta^2}+\frac{\partial^2 v_z}{\partial z^2}\right) \text{-------(4)}$$

Energy equation

$$\rho c_p\left(v_r\frac{\partial T}{\partial r}+\frac{v_\theta}{r}\frac{\partial T}{\partial \theta}+v_z\frac{\partial T}{\partial z}\right)=k\left(\frac{\partial^2 T}{\partial r^2}+\frac{1}{r}\frac{\partial T}{\partial r}+\frac{1}{r^2}\frac{\partial^2 T}{\partial \theta^2}+\frac{\partial^2 T}{\partial z^2}\right) \text{----------(5)}$$

Equations from (1) to (5) were solved for steady state cases by using of ANSYS-FLUENT-15. The specifications and initial and boundary conditions of the models that solved in this study displayed in table (2).

3. Experimental investigation

3.1 Water heating solar collector Specifications

A flat coil solar collector which used in this experimental investigations with single glass cover from for reducing the heat losses by convection and radiation with insulation to avoid the heat dissipation. The specifications of the present water heating solar collector are displayed in table (1).

3.2 Experimental setup and test procedure

The experimental tests conducted at Technical College at Al-Mussaib city-Iraq, located at $32^0$5' North latitude and $44^0$3' East longitude, this position taking as location for account in measuring the solar radiation intensity at title angle of $32.5^0$and weather conditions. Application was used to measured intensity solar radiation (I) with daily time, water volume flow rate, atmospheric temperature (T_a), inlet water temperature (Ti) and the outlet water temperature (To), inlet water prssure (Pi) and the outlet water pressure (Po). Temperatures, pressures and intensity solar radiation are variable with time and they obtained every 15 minutes from the measured values. The Experimental test rig includes flat coil water solar collector (FCSC) using a copper tubes as receiver is designed and fabricated in order to

examine the effect of different ambient and water flow conditions on the hydrothermal performance of collector. The experimental test rig shown in figure (2) was tested outdoor at Technical College in AL-Mussaib city-Babylon-Iraq for a period of March and April 2015. The schematic diagram of this complete experimental system is shown in the figure (3). The experimental tests rig consists of absorber flat coil tube which is made of copper which has specifications as given in the table (1). The absorbers surfaces are coated with mat black paint produced by Al-Marjan Company, Baghdad-Iraq. The collector frame which manufactured from rectangular steel tubes formed in a rectangular shape. The collector has a width of 2 m and a long of 1 m, the glass cover which is 3.5 mm thickness glass panel of 2040 mm x 1040 mm in dimensions, the gap between the glass and the absorber is 20 mm to minimize upward heat losses from the absorber tube, stationary Base frame has been designed and constructed in order to undergo the hard weather conditions, water pump which used are electric AC type to recirculate water, connecting pipes which a thermal insulated plastic pipes of (3/4 inch) are used to connect the different parts of the experimental setup, and A glass wool has a thickness of 30 mm was used as insulation.The steps approved before each experimental test included lift the cover of system which protects it from rain and dust, clean the glass cover of FCSC with cleanner fluid, connect all thermocoupes to data loggers, then ajusmented date and time recorder of data loggers, data from all thermocouples were recorded every 15 minutes then checked, ensure that all valves are open in the circulation path, pyranometer was cleaned from dust, solar radiation data was recorded every 15 minute by LOGBOX data logger, switch on the water pump to recirculate the water withen the system. The setup is a well instrumented solar collector system in which the water flowing inside the copper tube heated by solar energy. The water enters the receiver through the bottom connection and leaves the receiver at the top then flows to the insulated storage tank. Experiments are conducted for variable flow rate namely of (0.16, 0.2, 0.3, 0.4, 0.5, 0.6, 0.7, 0.8, 0.9, 1, 1.1) cubic meter per hour through the receiver for 11 clear and partly cloudy days on March 2015, then replication on April 2015.

4. Performance analysis

The value of instantaneous thermal efficiency η_{th} for the water solar collector has been calculated from the energy balance of the receiver which shown in the figure (1). The useful energy as heat gain (Qu) transported to the receiver defined as (Ma *et.al.*, 2011):

$$Q_u = mc_p(T_0 - T_i) \text{----------(6)}$$

Where: T_i and T_o represent the inlet fluid and exit fluid temperatures, respectively.

The instantaneous thermal efficiency of the water solar collector defined as the ratio of heat gain (Qu) supplied to Aa, and the solar radiation (I) which is incident on the area of aperture (Ma *et.al.*, 2011).

$$\eta = \frac{mc_p(T_0 - T_i)}{I \quad A_a} \text{----------(7)}$$

The pressure drop for single phase in flat coiled tubes calculated as (Ravigururajan, 1987):

$$\Delta P = \frac{f_c}{2} * \frac{L}{d} * \rho V^2 \text{----------(8)}$$

5. Instrumentation

5.1 Temperature measurements

Six thermocouples types (K) with 0.4 mm diameter are used in this work. These thermocouples are connected to Digital data logger type of 12 channels temperature recorder with SD card data logger model BTM-4208SD manufactured by Lutron company of Taiwan to read and record the magnitude of temperature with an accuracy of (±4%) as shown in figure (4). The temperature measurements range of (-50 to 999.9 ºC) and resolution of 0.1 ºC.

5.2 Solar radiation measurements

Solar intensity was measured with a Kipp and Zonen class one Pyranometer model CMP22 as shown in figure (5), which having a measuring range of up to 4000 W/m^2 (error<5 W/m^2). It was installed on the collector at tilt angle of 32.5 º with the horizontal. 8 channels data logger manufactured by Kipp and Zonen Company, Delft, Netherland model LOGBOX SD as shown in figure (6) was used to record the data every ten minute in W/m^2. The LOGBOX SD has ability to print the measured values of the solar radiation intensity at different specific time periods.

5.3 Wind speed measurements

The wind speed was measured by using a Lutran multifunctional anemometer device model (ABH-4225) made in Taiwan, with an accuracy of (±3%). The measurement range of the anemometer is (0.4-30 m/s) and resolution of 0.1 m/s as shown in figure (7).

6. Error analysis

In the present work, Kline and McClintock (Holman, 1994) procedure is used to evaluate the percentage error of the experimental work. The root mean square error in a measured quantity is calculated by the following formula:

$$\delta R = \sqrt{\left(\sum_{m=1}^{n} \frac{\delta R}{\delta X_m} \delta X_m\right)^2} \quad \text{----------(9)}$$

where:

R is the calculated quantity and X is the measured variable.

δR is the error of the calculated quantity

δX is the error of the measured variable

7. Results

7.1 Theoretical Results

The scaled residuals of the solved models are found that the solution of first model is converged at 531 iterations during 2 hour and the solution of second model is converged at 1197 iterations during 2.5 hours. Figures (8) and (9) show the contour of the water temperature, the results data show that the water temperature is increased along tube length due to heat addition from the tube wall. It is found the difference of temperature for the first model is 1.34 °C, while 0.77 °C for the second model for all models for all models. Figures (10) and (11) show the contour of the static pressure for all models. Higher pressure in tube inlet is indicated, while lower pressure at tube outlet for all models. It is found the pressure drop for the first model is 29600(Pa), while 68500 (Pa) for the second model. These computational obtained results show the pressure drop along the receiver within the second model is higher than it for the first model. The profiles of velocity and temperature at tube outlet are shown in figures (12) and (13). The computational Thermal efficiency and its factors are given in table (5.6) for all models.

7.2 Experimental Results

Figure (14) shows the hourly variation of incident solar radiation, ambient temperature, and wind speed for selected clear days for experimental tests. The incident solar radiation was measured with a Kipp and Zonen Pyranometer model

CMP22 installed on the collector at 32.5 º with the horizontal. The sample of hourly weather data are measured by weather measurement devices mounted on the collector place shown in table (4). Figure (15) displays the hourly time variation for the measured values of water outlet and inlet temperatures, and ambient temperature for clear days on 17th March and 8th April 2015 for the same water flow rate of 0.7 m^3ph. It is showed the maximum differences of temperatures are 2 ºC at 12:30 pm and 1.2 ºC at 12:30 pm, respectively. It is found that the maximum difference of temperature for clear day on March is higher than it for clear day on April day due to increasing of solar radiation energy that absorbed.

Figure (16) represents a sample of the hourly variation of the heating performance which includes solar heat flux, useful heat, and thermal efficiency for clear day on 5th April, 2015. The Solar heat flux calculated as:(Duffei, 1991)

$$q_{flux} = A_a \times I \text{ ----------(10)}$$

Figure (17) shows the hourly variation of the water outlet temperature on April, 2015 for all tests days. It showed the exit temperature of water increased till 16:00 pm and the maximum temperature is 72 ºC with 0.2 m^3ph water flow rate for clear day on 2nd April, 2015. Figure (18) shows the hourly variation of the thermal efficiency on April, 2015 for all tests days. It showed the thermal efficiency increased till 14:30 pm and the maximum thermal efficiency is 81.6% with 0.3 m^3ph water flow rate for clear day on 7th April, 2015. Figures (19) and (20) show the hourly variation of the difference of temperatures between inlet and outlet of receiver on March and April, 2015 respectively for all tests days. It showed the maximum temperature differences are 3 ºC for clear day on 10th March and 4 ºC for clear day on 2nd April, 2015. Figures (21) and (22) show the hourly variation of the water temperature inside the storage tank on March and April, 2015 respectively for all tests days. It showed the maximum temperatures are 70.5 ºC for clear day on 10th March and 71 ºC for clear day on 2nd April, 2015. The operation curve for the tests in clear days is shown in figures (23) and (24). The thermal efficiency of the FCSC system was determined by calculating the instantaneous efficiency for high values of incident solar radiation, bulk temperature of working fluid in the inner tube, ambient temperature. This needed experimentally measured of the incident solar radiation onto FCSC as well as the energy rate addition to the working fluid under quasi-steady state conditions. That's occurs over the period from 10:30 am to 14:30 pm. The value of intersection of the efficiency line with the vertical axes is 56 %. The thermal efficiency varies linearly with values of (Ti-Ta)/I. This relationship between the thermal efficiency and (Ti-Ta)/I can be expressed as:

For March 2015

$$\eta_{th} = 0.575 - 6.032\left(\frac{Ti-Ta)}{I}\right) \text{ ----------(11)}$$

For April 2015

$$\eta_{th} = 0.547 - 3.92\left(\frac{Ti-Ta)}{I}\right) \text{ ----------(12)}$$

The variation of friction factor with Reynolds Number on April, 2015 is shown in figure (25). It is found that the maximum friction factor is 0.77 and the minimum friction factor is 0.001. The numerical results are compared with experimental results and gave a good agreement as shown in table (3). The present work is compared with the results of results in Reference (1), which represented water flat straight solar collector with 20 (L/min) water flow rate for water temperature inside storage tank as shown in Fig. (26), it is found that the present flat coil solar collector is more efficient than the flat straight solar collector. Comparison between the present work and Reference -1 gave increasing of 12.3 % for water inside storage tank.

8. Conclusions

The performance of Flat Coiled tube Solar Collector (FCSC) using of a flat coiled tube as receiver investigated numerically and experimentally under outdoor conditions. The numbers of successful tests were 22 tests. The conclusions can be extracted from this paper include; The present FCSC collector affected by major parameters includes variable water volume flow rates through the receiver, incident radiation and temperature of ambient. Increasing incident radiation and ambient temperature lead to improvement on thermal performance of the present collector, a maximum difference of temperature between outlet and inlet of collector was (4º C) at (13:00 pm) for clear day on 2nd April, 2015, while a maximum useful heat gain was (1300 W) at (13:00 pm) for clear day on 2nd April, 2015, the thermal efficiency of the collector is increasing with the increasing of solar radiation. The collector efficiency ranged from (10% to 81.6 %) %), the maximum water temperatures at receiver outlet and storage tank are 72 ºC and 71 ºC respectively on for clear day on 2nd April, 2015, the maximum value of friction factor of flat coiled tube is 0.77.

References

Alireza Hobbi , Kamran Siddiqui, 2009 "Experimental study on the effect of heat transfer enhancement devices in flat-plate solar collectors" International Journal of Heat and Mass Transfer 52 ,4650–4658. Elsevier.

Bird R. B., Armstrong R. C., and Hassager O. , 1987 ,Dynamics of Polymeric Fluids: Volume 1 Fluid Mechanics, Wiley: NY.

Bird R. B., Stewart W. E., and Lightfoot E. N. , 2002 Transport Phenomena,2nd edition, Wiley: NY.

Cadafalch J. ,2009"A detailed numerical model for flat-plate solar thermal devices" Solar Energy 83 ,2157–2164. Elsevier.

Duffie, J.A., Beckman, W.A., 1991. Solar Engineering of Thermal Processes, second ed. Wiley Inter science, New York.

Holman J.P. 1994. "Experimental methods for engineers". McGraw-Hill,Inc.,New York

Ma J., Sun W., Ji J., Zhang Y., Zhang A., and Fan W.,2011"Experimental and theoretical study of the efficiency of a dual function solar collector". Applied Thermal Engineering; 31: 1751–1756.

Madhukeshwara. N, Prakash E. S. 2012,"An investigation on the performance characteristics of solar flat plate collector with different selective surface coatings" International Journal of Energy and Environment, Volume 3, Issue 1, pp.99-108.

Mahmud Jamil Muhammad, Isa Adamu Muhammad, Nor Azwadi Che Sidik, Muhammad Noor AfiqWitri Muhammad Yazid 2016 "Thermal performance enhancement of flat-plate and evacuated tube solar collectors using nanofluid: A review" International Communications in Heat and Mass Transfer May

Molero Villar N., Cejudo Lo´pez J.M. , Domı´nguez Mun˜ oz F., Rodrı´guez Garcı´a E., Carrillo Andre´s A. ,2009,"Numerical 3-D heat flux simulations on flat plate solar collectors" Solar Energy 83,1086–1092 . Elsevier.

Raja Sekhar Y., Sharma K. V. and Basaveswara Rao M. ,2009 "Evaluation of heat loss coefficients in solar flat plate collectors" Journal of Engineering and Applied Sciences Vol. 4, No. 5, July , ISSN 1819-6608 ARPN

Soteris A. ,2004, Kalogirou solar thermal collectors and applications, Prog. Energy 640 Combust. Sci. 30 ,231–295.

Tiruvadi Srinivasa Ravigururajan ,1986,"General correlations for pressure drop and heat transfer for single-phase turbulent flows in ribbed tubes" Thesis, Iowa State University

Table (1): PTC specifications

parameter	Value/type
Collector aperture area	2 m^2
Aperture width	2 m
Aperture length	1 m
Copper tube length	12 m
Tube wall thickness	0.90 mm
Tube diameter	17.2 mm
Tracking model	stationary
Storage tank	60 Liter

Table (2): Specification of initial and boundary conditions.

Model No.	Flow rate (m^3ph)	Mean inlet velocity (m/s)	Inlet Temperature (°C)	Wall heat flux (W)	Flow Regime
1	0.6	0.7	45	1840	Turbulent
2	1.1	1.31	49	1505	Turbulent

Table (3): A typical results of ANSYS Fluent software with corresponding experimental results for flat coiled tube.

Model No	Parameter	Experimental	Theoretical
1	Ti (° C)	45	45
	To (° C)	46	46.33
	Efficiency (%)	46.6	49.8
	Heat flux(W)	1840	1840
	Heat absorbed (W)	857	918
2	Ti (° C)	49	49
	To (° C)	49.7	49.76
	Efficiency (%)	58.7	63.7
	Heat flux(W)	1505	1505
	Heat absorbed (W)	884	960

Table (4): Claimed condition for many days of test.

	6-March-2015			19-March-2015			23-March-2015		
Time (hr)	I (W/m^2)	T_a (ºC)	wind speed (m/s)	I (W/m^2)	T_a (ºC)	wind speed (m/s)	I (W/m^2)	T_a (ºC)	wind speed (m/s)
8	300	15.2	0.4	500	12	2.7	300	14	1
8.5	380	16.3	0.2	600	12.9	0.7	350	16	0.6
9	456	20.1	0.7	693	20.5	1.8	400	18	1.4
9.5	593	22.5	0.3	781	21.8	0.8	455	20.5	2.3
10	676	22.2	0.4	860	22.7	0.6	552	22.3	1.9
10.5	747	25.1	0.7	894	23.8	0.7	744	24.4	2.3
11	770	25.9	1.5	943	25.1	2.2	807	25.4	2.2
11.5	779	27.9	0.7	965	26.1	2	908	26.3	1.5
12	784	27.1	0.5	948	26.9	1.2	885	26.5	2.4
12.5	770	28.1	0.5	932	27.3	3	881	27	1.8
13	763	24.3	1.1	891	27	0.4	862	26.9	1.2
13.5	712	26.7	1.5	816	26.7	0.9	830	26.8	1.5
14	655	26.3	2.3	752	26.7	3.1	772	26.5	1.8
14.5	584	27.6	0.7	655	24.2	3.9	719	26.1	2
15	489	26	0.7	553	24.3	2	630	24.2	2.2
15.5	392	24	1.5	424	25.6	0.7	470	22	1.8
16	280	22	2.7	282	26.5	0.4	365	20	1.5

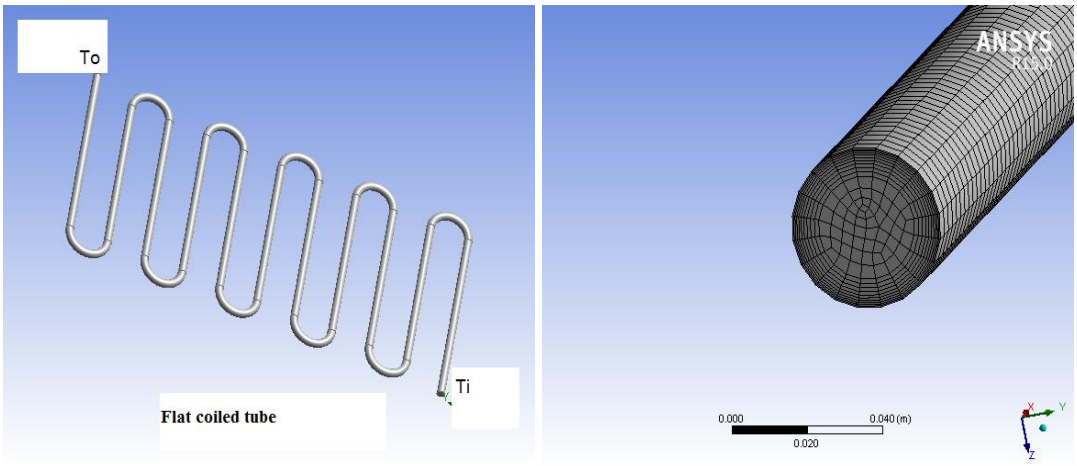

a b

Fig. (1): Geometry and mish of the receiver (flat coiled tube).

Fig.(2): The complete experimental rig.

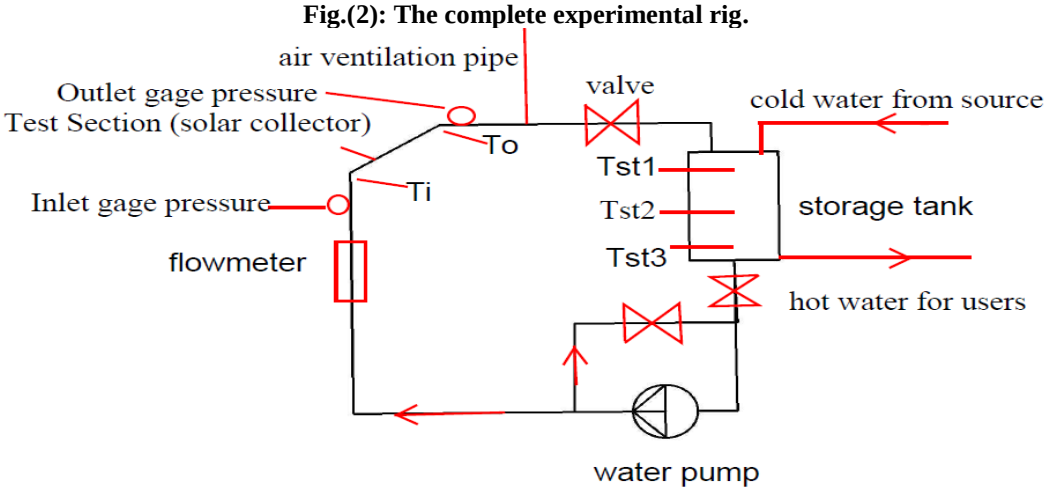

Fig.(3): A schematic diagram of the complete experimental set-up.

Fig.(4): Digital data logger type (12 channels temperature recorder Lutron, model BTM-4208SD.

Fig.(5): Pyranometer model CMP22

Fig.(6): An 8 channels data logger

Fig.(7):Lutran anemometer device.

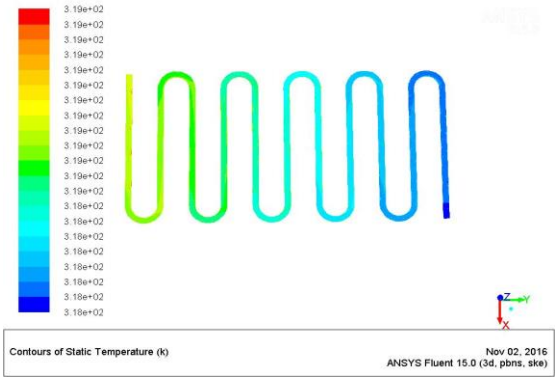

Fig.(8):Contours of static temperature of model-1

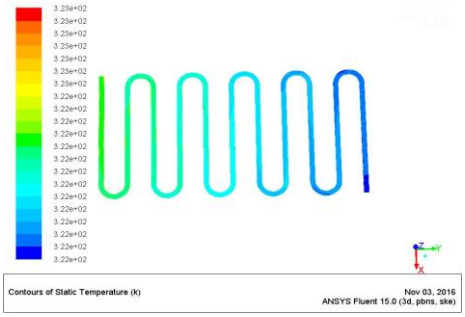

Fig.(9):Contours of static temperature of model-2

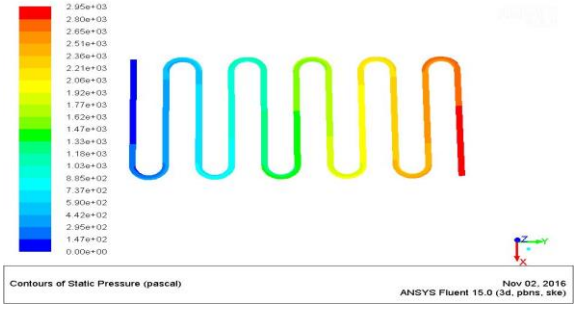

Fig.(10):Contours of static pressure of model-1.

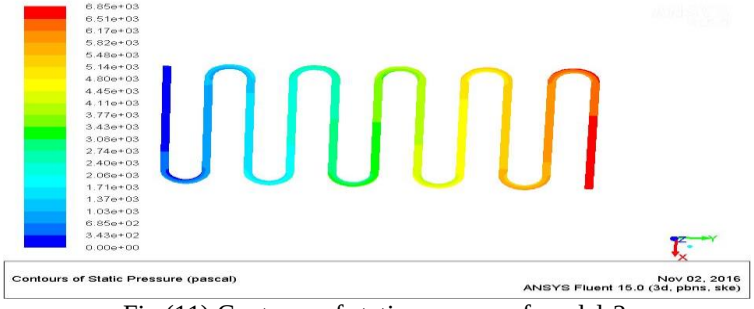

Fig.(11):Contours of static pressure of model-2.

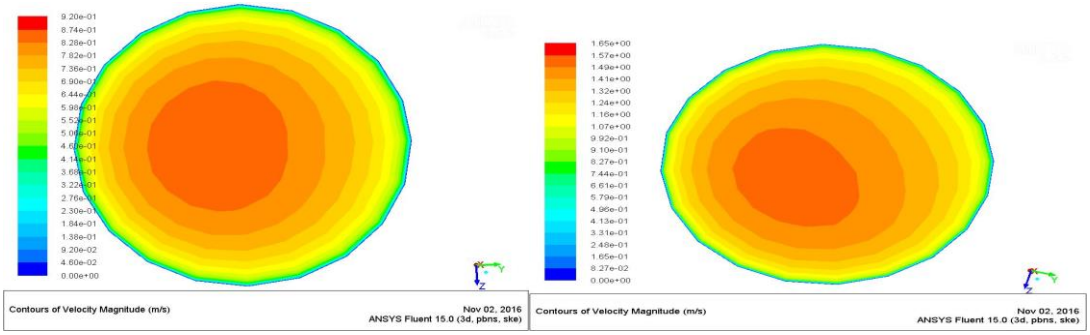

Model-1 Model-2

Fig.(12):Contours of velocity magnitude profile at tube outlet

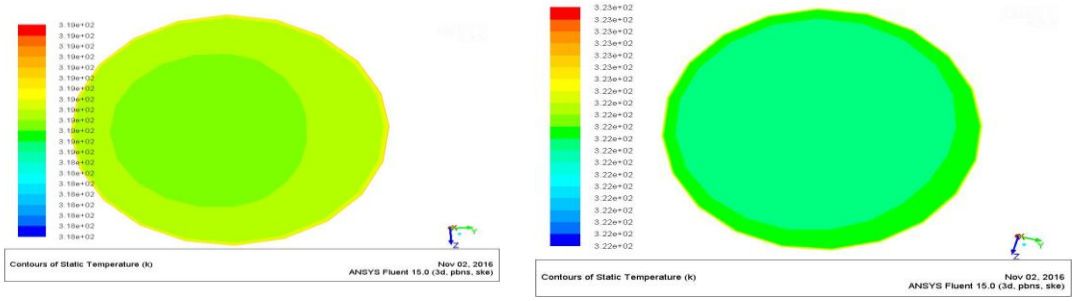

Model-1 Model-2

Fig.(13):Contours of static temperature profile at tube outlet.

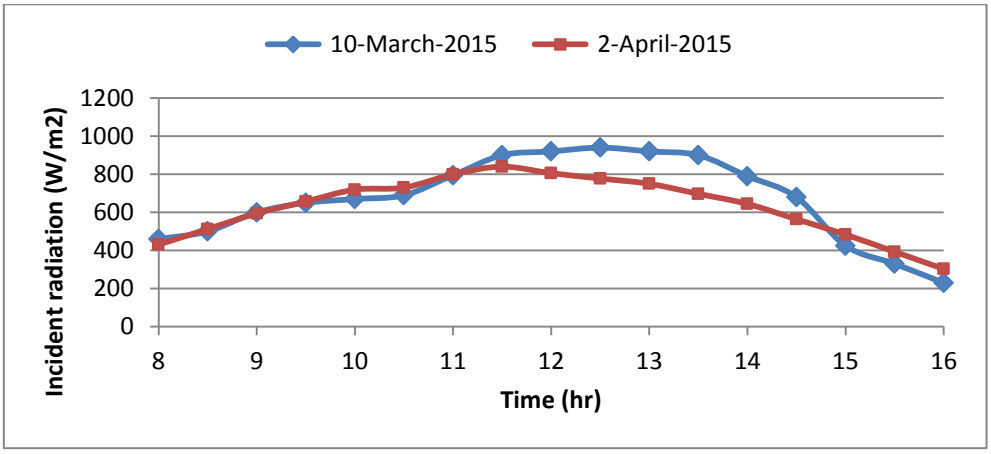

a

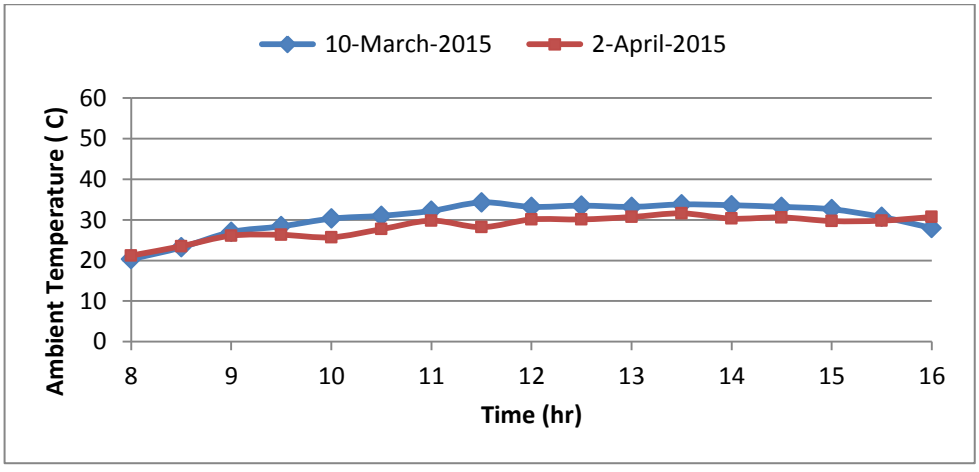

b

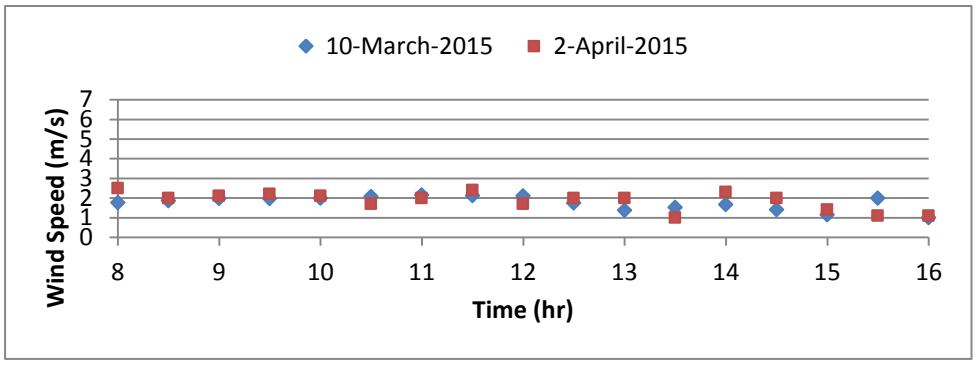

c

Fig.(14): Hourly measured Data for (a) Incident radiation on the collector, (b) Ambient temperature, and (c) Wind Speed for clear days on 10 th of March and 2 nd of April, 2015

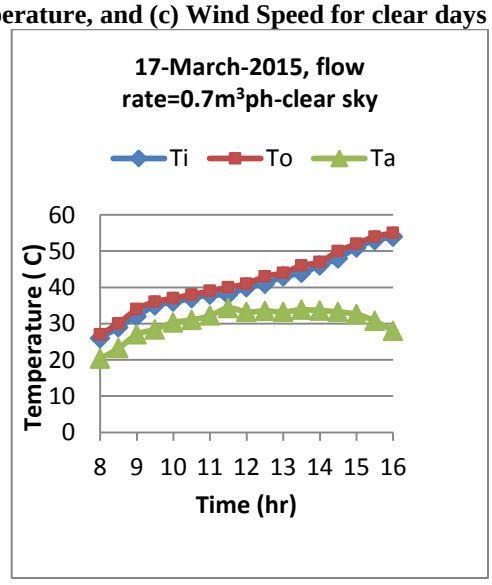

a

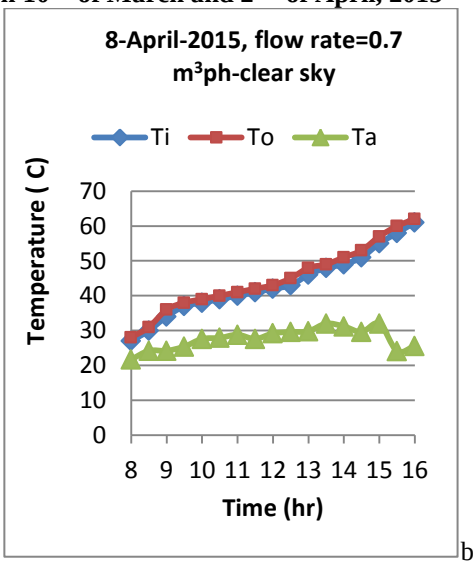

b

Fig.(15): Hourly measured inlet, outlet and ambient temperatures` for (a) clear day and 17th March,2015, (b) clear day on 8th April 2015.

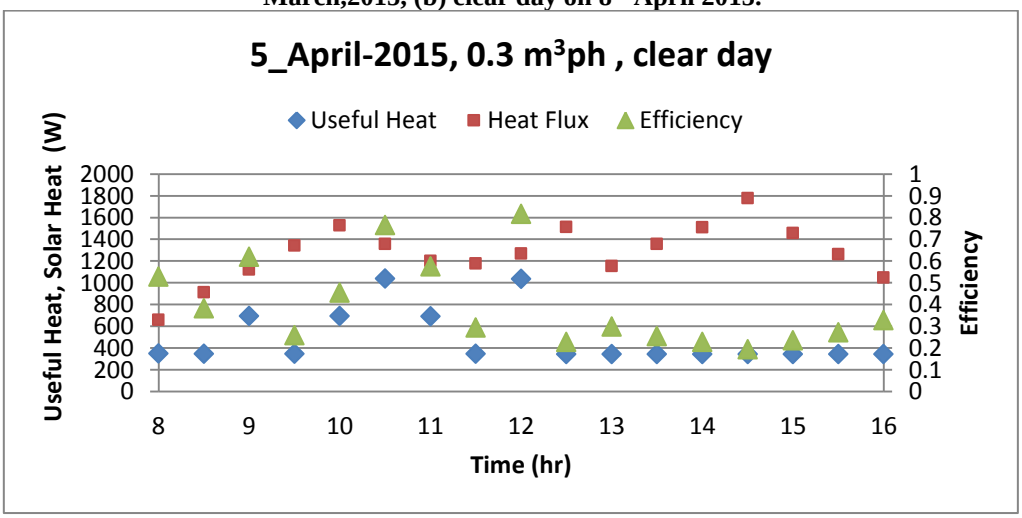

Fig.(16): Hourly measured useful heat, solar heat, and efficiency for clear days on April,

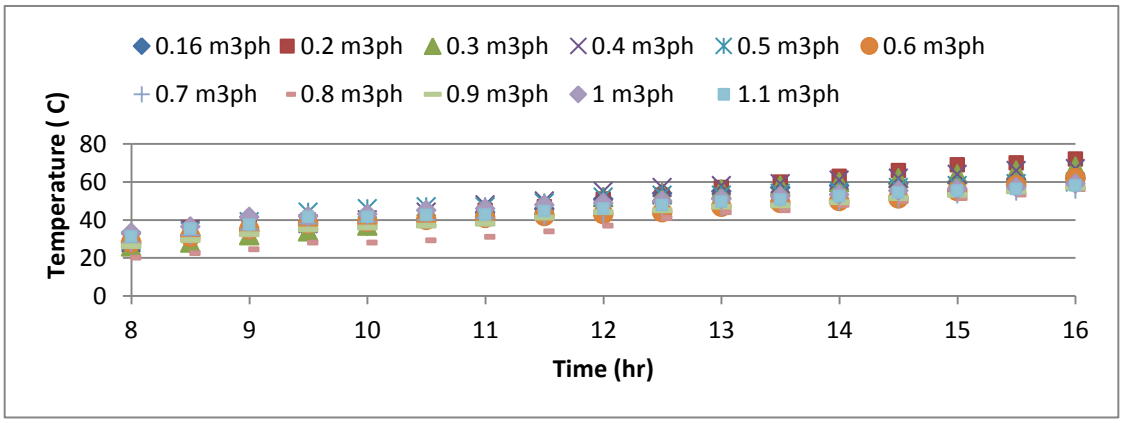

Fig.(17): Hourly measured outlet Temperature for all test days on April, 2015.

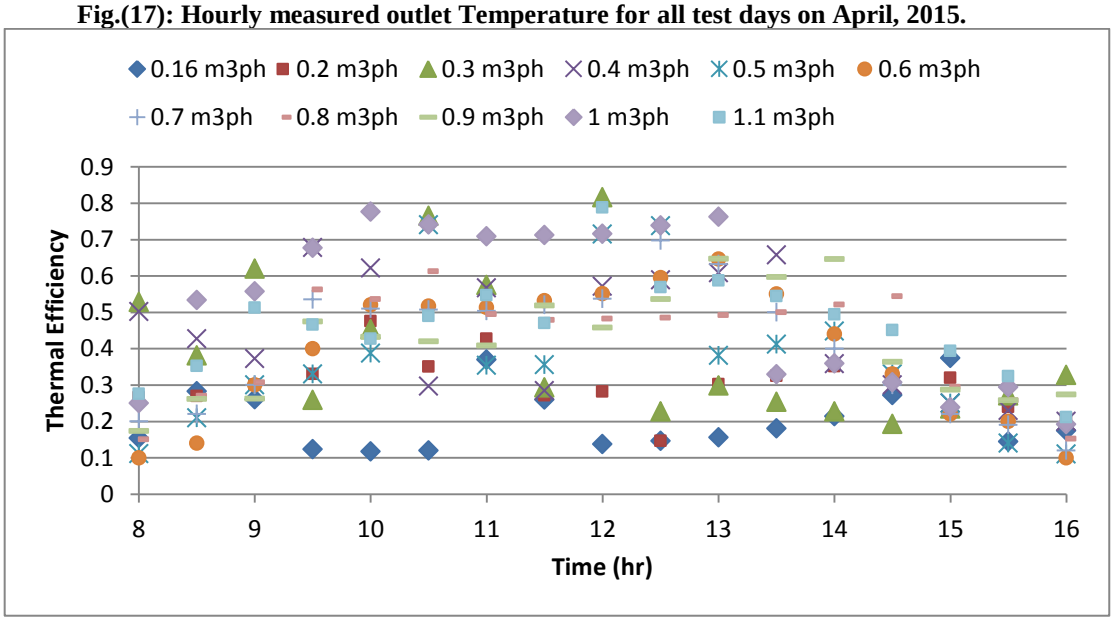

Fig.(18): Hourly efficiency on April, 2015.

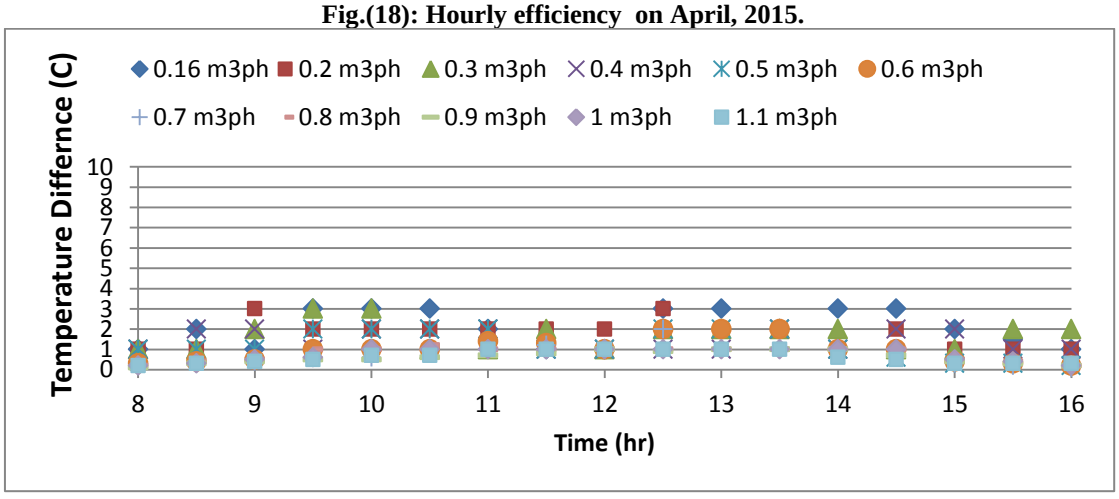

Fig.(19): Hourly measured temperature difference on March, 2015.

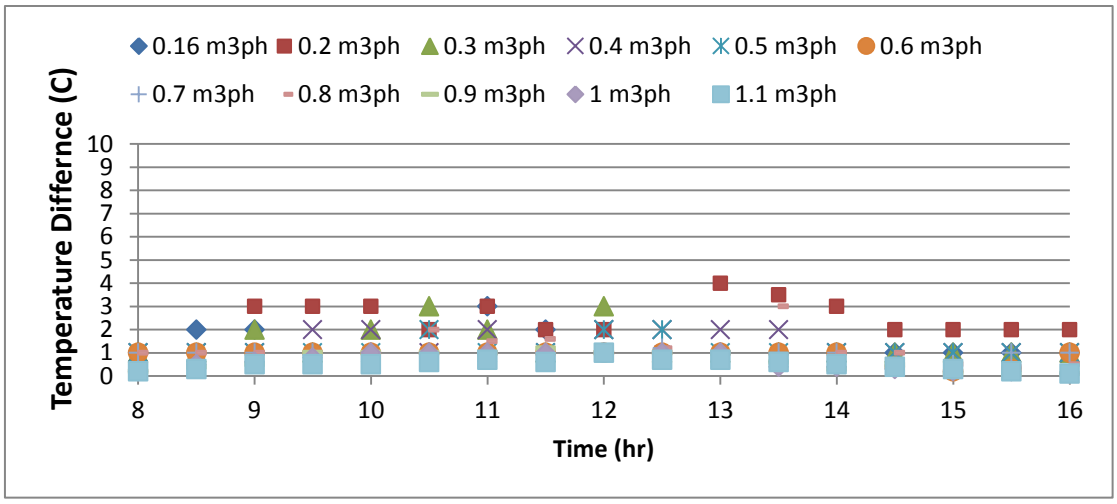

Fig.(20): Hourly measured temperature difference on April, 2015.

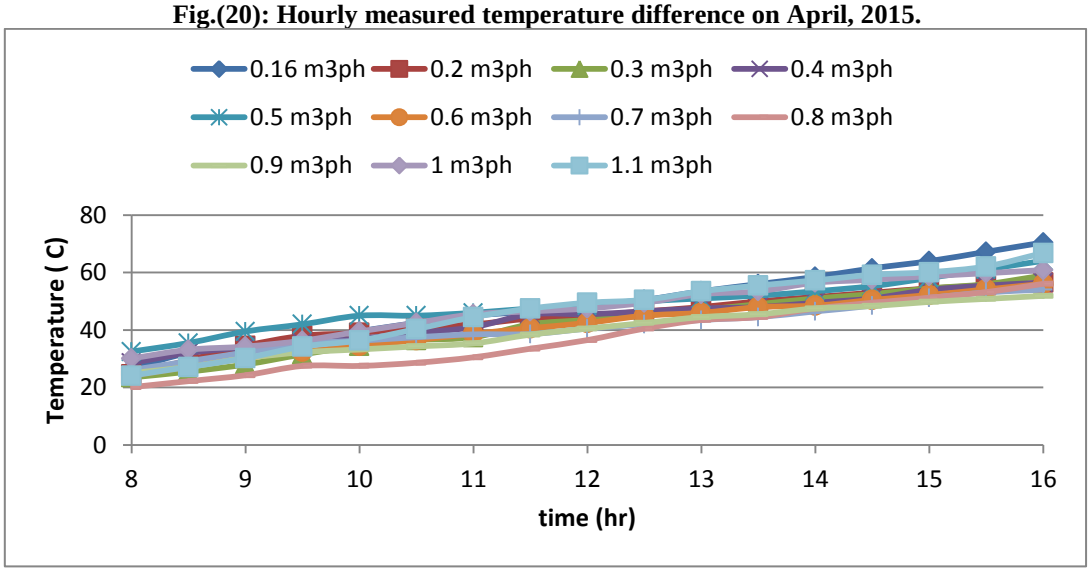

Fig.(21): Storage Tank Temperature March, 2015

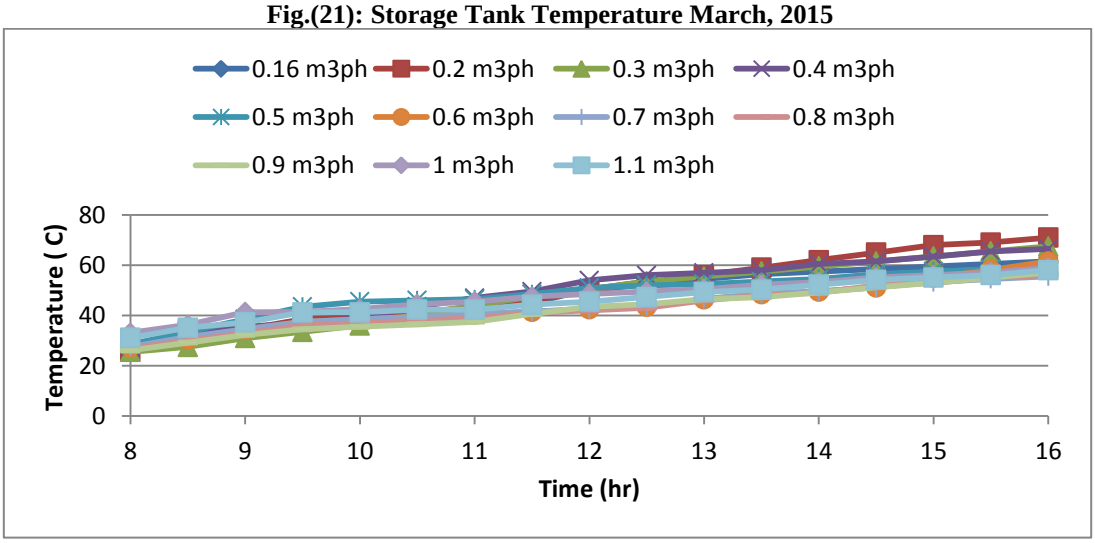

Fig.(22): Storage Tank Temperature April, 2015

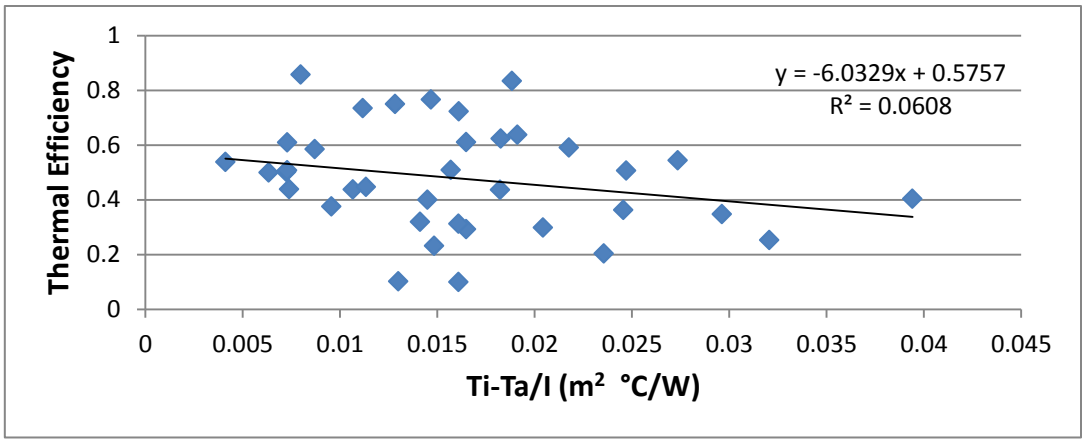

Fig.(23): Operation Curve for clear days on March, 2015.

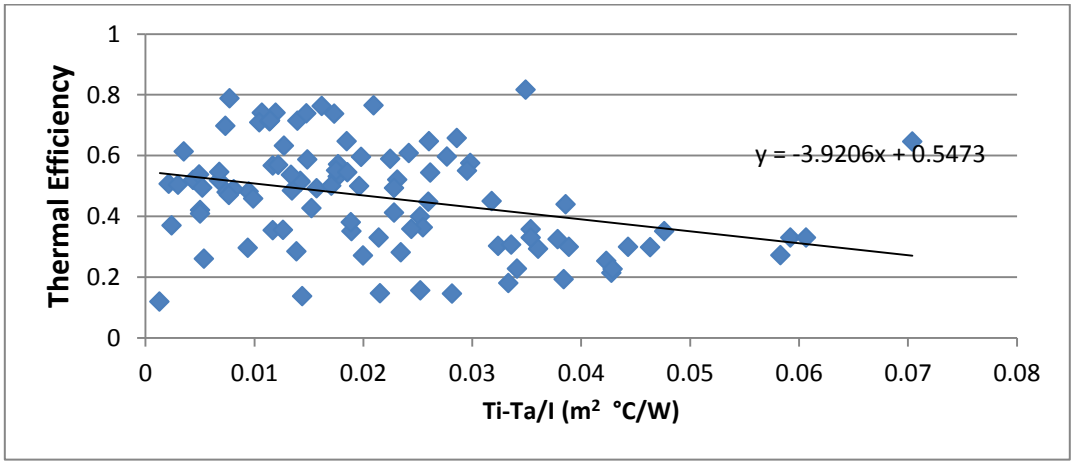

Fig.(24): Operation Curve for clear days on April, 2015.

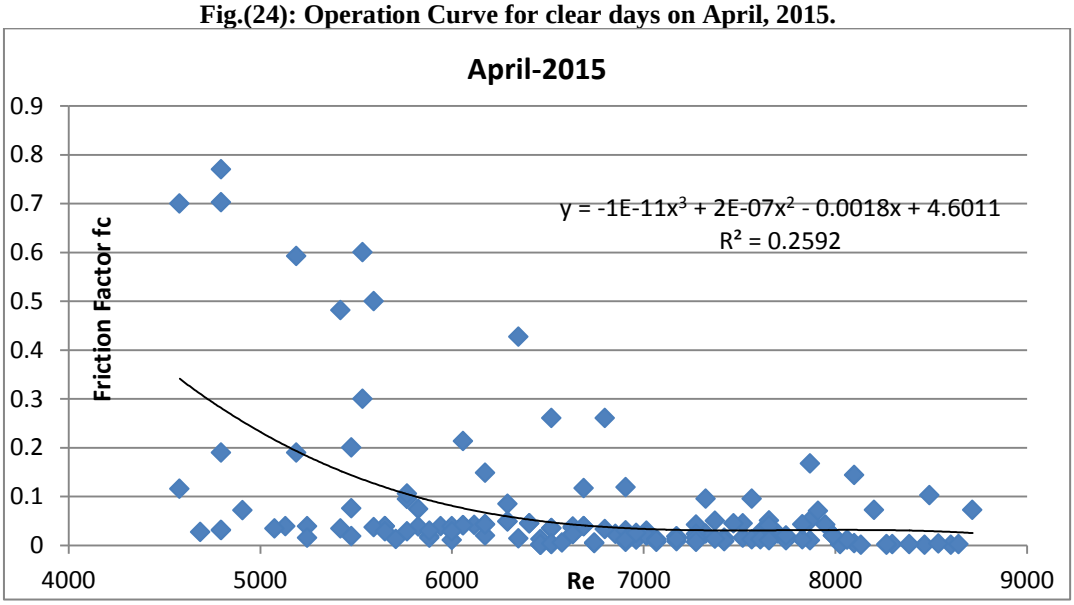

Fig.(25): Friction factor with Reynolds Number on April, 2015.

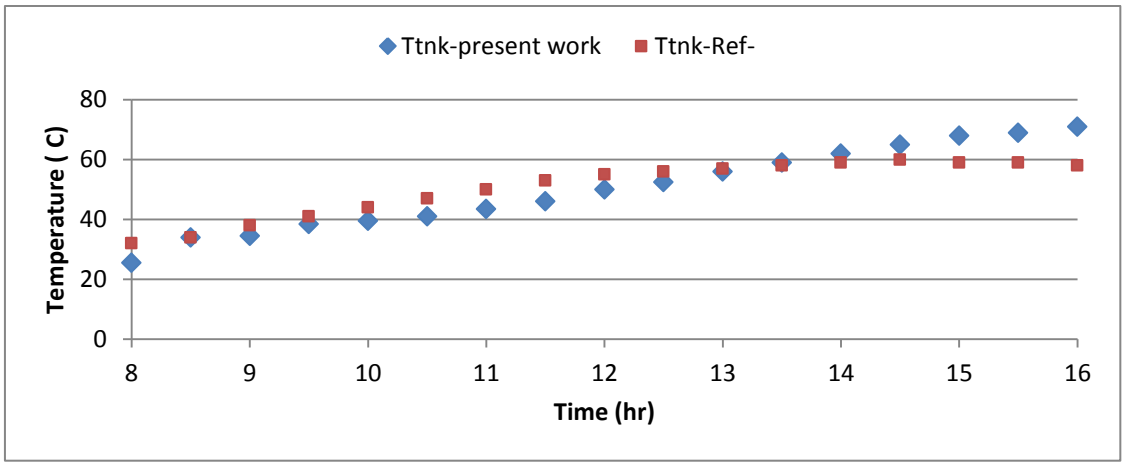

Fig.(26): Comparison between the present work and Reference (Madhukeshwara, 2012) for water inside storage tank.